Supplementary materials for
Quantum Sensors for Microscopic Tunneling Systems

Alexander Bilmes*,[1] Serhii Volosheniuk,[1] Jan David Brehm,[1] Alexey V. Ustinov,[1,2,3] and Jürgen Lisenfeld[1]

[1)] *Physikalisches Institut, Karlsruhe Institute of Technology, 76131 Karlsruhe, Germany*[a)]

[2)] *National University of Science and Technology MISIS, Moscow 119049, Russia*

[3)] *Russian Quantum Center, Skolkovo, Moscow 143025, Russia*

(Dated: 29 November 2020)

SUPPLEMENTARY METHODS

Sample capacitor design

The choice of the sample capacitor dimensions (in plate geometry) is a trade-off between the participation ratio of the sample dielectric which influences the qubit coherence, and the dielectric thickness d which determines the typical coupling strength of the qubit to sample TLS. As explained in the main text, we chose $d = 50$ nm to balance the TLS-qubit coupling strength g against an expected qubit energy relaxation time of $T_1 \approx 1\,\mu s$. Further, to determine the maximum sample capacitor area A, we consider the qubit's energy relaxation rate expressed in terms of dielectric losses contributed by the overlap capacitor:

$$\Gamma_1 = 2\pi f_{01} \cdot p_{\mathrm{s}} \cdot \tan\delta_0 + \Gamma_{1,0}. \tag{1}$$

Here, $\tan\delta_0$ is the loss tangent of the sample dielectric, and $\Gamma_{1,0}$ combines all other sources of loss. The sample capacitor's participation ratio $p_{\mathrm{s}} = C_{\mathrm{s}}/(C_{\mathrm{s}} + C)$ is defined as the electric energy stored in the sample capacitor divided by the total energy of the qubit. Here, $C_{\mathrm{s}} = \varepsilon_0\varepsilon_{\mathrm{r}}A/d$ is the sample capacitance, and C is the sum of all other capacitors shunting the qubit's Josephson junctions. Assuming an energy relaxation rate $\sim 1/(10\,\mu\mathrm{s})$ of the qubit without a sample capacitor, and the loss tangent of 1.6×10^{-3} in AlO_x[1], we arrived at a sample capacitor size of $(300\,\mathrm{nm} \times 2.1\,\mu\mathrm{m})$ used in the first generation of samples. As reported in Chap. 4.1 of AB's thesis [2], these samples were used to deduce a loss tangent of $\tan\delta_0 = 1.7 \times 10^{-3}$ of the employed aluminum oxide. To improve the signal-to-noise ratio for TLS spectroscopy, the sample capacitor size $(250\,\mathrm{nm} \times 300\,\mathrm{nm})$ of the second sample generation was designed for a reduced Γ_1 of $1/(3\,\mu\mathrm{s})$, following Eq. (1) and values of $\Gamma_{1,0} \sim 1/(5\,\mu\mathrm{s})$ and $\tan\delta_0$ measured with the first generation samples.

Measuring the electric dipole moments of sample TLS

As mentioned in the main text, the sample TLS are identified by their tunability via the DC-voltage V_{s} maintained across the sample capacitor, while they do not respond to the globally applied DC-electric field generated by the gate placed above the microchip. As a note, the simulated distribution of the global field[2] shows that all detectable TLS which reside at qubit circuit interfaces other than in the Josephson junction or in the sample capacitor, are exposed to the global field. Moreover, the TLS hosted in the qubit's Josephson contacts are not tunable by V_{s} since the qubit's island has a constant DC-electric potential due to the transmon regime.

From a fit to the hyperbolic dependence of the TLS' resonance frequency $f = \sqrt{\Delta_0^2 + (\varepsilon_{\mathrm{i}} + \gamma_{\mathrm{s}}V_{\mathrm{s}})^2}/\mathrm{h}$ on the applied voltage V_{s}, we extract the tunability coefficient γ_{s} which is related to the TLS' electric dipole moment component $p_{\parallel}$ parallel to the field by $\gamma_{\mathrm{s}}V_{\mathrm{s}} \equiv 2p_{\parallel}V_{\mathrm{s}}/d$. The latter term corresponds to the dipole energy in the electric field V_{s}/d which adds to the intrinsic asymmetry energy ε_{i}. The cumulative spectral density of sample TLS, which is plotted vs. the deduced dipole moment size in Fig. **S1**, is comparable to previous reports[1–4].

The voltage V_{s} was controlled via an attenuated coaxial RF line whose warm end was connected to a voltage source (output voltage $\widetilde{V}_{\mathrm{s}}$), and the cold end was connected to the sample capacitor's top electrode. This RF line consisted a chain of following

---

[a)] e-Mail: alexander.bilmes@kit.edu

elements: a $-20\,\mathrm{dB}$ attenuator at room temperature, $\sim 50\,\mathrm{cm}$ stainless-steel (SS) coaxial cable leading to the $4\,\mathrm{K}$ plate, two $-10\,\mathrm{dB}$ attenuators at $4\,\mathrm{K}$, further $\sim 30\,\mathrm{cm}$ of SS coax leading to a $-10\,\mathrm{dB}$ at the still plate, and another $\sim 15\,\mathrm{cm}$ Cu-coax leading to a $-3\,\mathrm{dB}$ attenuator at the mixing chamber. We have measured at ambient conditions the voltage drop V_s between the $-3\,\mathrm{dB}$ attenuator's central pin and ground as function of $\widetilde{V}_\mathrm{s}$, and found a division factor of $\widetilde{V}_\mathrm{s}/V_\mathrm{s} = 205$.

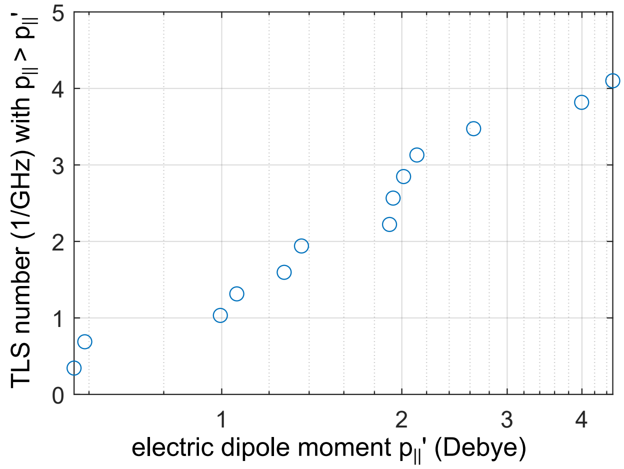

FIG. **S1**. Electric dipole moment sizes of TLS hosted in the AlO_x sample dielectric. Data comprises measurements on two qubits.

Calculating the TLS spectral density

Here, we qualitatively describe our method to deduce the spectral TLS density from data sets such as that shown in the figure 2 **a** of the main text. A quantitative description can be found in chapter 4.2.4 of the PhD thesis by AB[2].

The data set of TLS spectroscopy, such as that shown in Fig. 2 **a**, shows estimates of the qubit's T_1-time (see color bar) as a function of its resonance frequency (vertical axis). Each trace along frequency is obtained using the swap spectroscopy protocol shown in the inset of **a** while one of the control voltages (piezo, DC-electrode or sample capacitor) is swept (horizontal axes). The TLS spectral density is the average number of TLS detectable per one such data trace. For each observed TLS, we calculate its spectral density by relating the control voltage range in which its trace is observed to the whole voltage range. The spectral density of a given class of TLS shown in **b** then is the sum over the spectral densities of individual TLSs which belong to this class.

As an example, take the data set shown in Fig. 2 **a**. If a TLS appears in all segments (plot regions with green, blue or red horizontal axes), then its spectral density is one over the observed frequency range, thus $1/(0.9\,\mathrm{GHz})$, as in the case of the violet-colored TLS trace. As an opposite example, the yellow highlighted TLS trace in the fourth segment from left is visible in only 50% of the data traces in this segment. Thus, its spectral density is $0.5/8/(0.9\,\mathrm{GHz})$ where $0.5/8$ is the relative part of all eight segments where the TLS is visible. The red colored trace partially appears in four segments, and accordingly the spectral density of this TLS is $(0.3+1+1+0.7)/8/(0.9\,\mathrm{GHz})$.

Characterization of interacting TLS

Here, we describe the model of interacting TLS used to fit the data shown in Fig. 3 of the main text. A more detailed description of the same model is given in Lisenfeld et al.[5] and its supplementary material.

The Hamiltonian of a single TLS is written as

$$H_i = \frac{1}{2}\varepsilon_i(V_\mathrm{p}, V_\mathrm{s}, V_\mathrm{g})\sigma_{\mathrm{z},i} + \frac{1}{2}\Delta_i\sigma_{\mathrm{x},i} = \frac{1}{2}E_i(V_\mathrm{p}, V_\mathrm{s}, V_\mathrm{g})\,\widetilde{\sigma}_{\mathrm{z},i}, \tag{2}$$

where Δ_i is the tunneling energy and the asymmetry energy $\varepsilon_i(V_\mathrm{p}, V_\mathrm{s}, V_\mathrm{g}) = \varepsilon_{i,0} + \gamma_{\mathrm{p},i}V_p + \gamma_{\mathrm{s},i}V_\mathrm{s} + \gamma_{\mathrm{g},i}V_\mathrm{g}$ depends linearly on external strain (set by the piezo voltage V_p), on the local electric field (controlled by the voltage V_s), and on the global electric field (set by V_g). Here, we use the tilde to distinguish operators such as the Pauli-matrices $\widetilde{\sigma}$ in the eigenbasis from those in the localized basis σ that is spanned by the two positions of the tunneling entity. The energy splitting in the diagonal basis is $E_i(V_\mathrm{p}, V_\mathrm{s}, V_\mathrm{g}) = \sqrt{\varepsilon_i^2(V_\mathrm{p}, V_\mathrm{s}, V_\mathrm{g}) + \Delta_i^2}$.

The interacting TLS system is described by the interaction Hamiltonian $H_\mathrm{T} = H_1 + H_2 + H_{12}$, with the coupling terms

$$H_{12} = g\,\sigma_{\mathrm{z},1}\,\sigma_{\mathrm{z},2}/2. \tag{3}$$

In the diagonal basis, the interaction Eq. (3) consists of four terms, which are combinations of $\widetilde{\sigma}_\mathrm{z}$ and $\widetilde{\sigma}_\mathrm{x}$ for each TLS. The resulting Hamiltonian, $\widetilde{H}$, can be significantly simplified[5] by neglecting all coupling terms of the form $\propto \widetilde{\sigma}_x\widetilde{\sigma}_z$ and $\propto \widetilde{\sigma}_z\widetilde{\sigma}_x$. They represent a coupling where one partner changes its state depending on the instantaneous state of the other subsystem and contribute only as small energy offsets. The significant parts of the interaction Hamiltonian using the longitudinal and transversal coupling factors g_z and g_x are thus

$$\widetilde{H}_{12} = \frac{1}{2}(g_\mathrm{z}\widetilde{\sigma}_{\mathrm{z},1}\widetilde{\sigma}_{z,2} + g_\mathrm{x}\widetilde{\sigma}_{x,1}\widetilde{\sigma}_{x,2}). \tag{4}$$

To characterize the interacting system, we first measure the TLS' tunneling energies Δ_i and the dependence of their asymmetry energies ε_i on the applied local E-field using swap-spectroscopy acquired in a wider frequency range as shown in Fig. **S2**. Next, the coupling strength of TLS 1 to the applied mechanical strain $\gamma_{\mathrm{p},1}$ is obtained from swap-spectroscopy scans taken at different strain values using data as shown in Fig. 3 of the main text. We obtain the remaining parameters $\gamma_{\mathrm{p},2}$, g_z, and g_x by fitting these data sets to a quantum simulation of the system Hamiltonian implemented with the QuTip software package[6]. Table I summarizes the resulting TLS parameters. The obtained coupling strengths are $g_\mathrm{z} \approx 25.0$ MHz, and $g_\mathrm{x} \approx -19.0$ MHz.

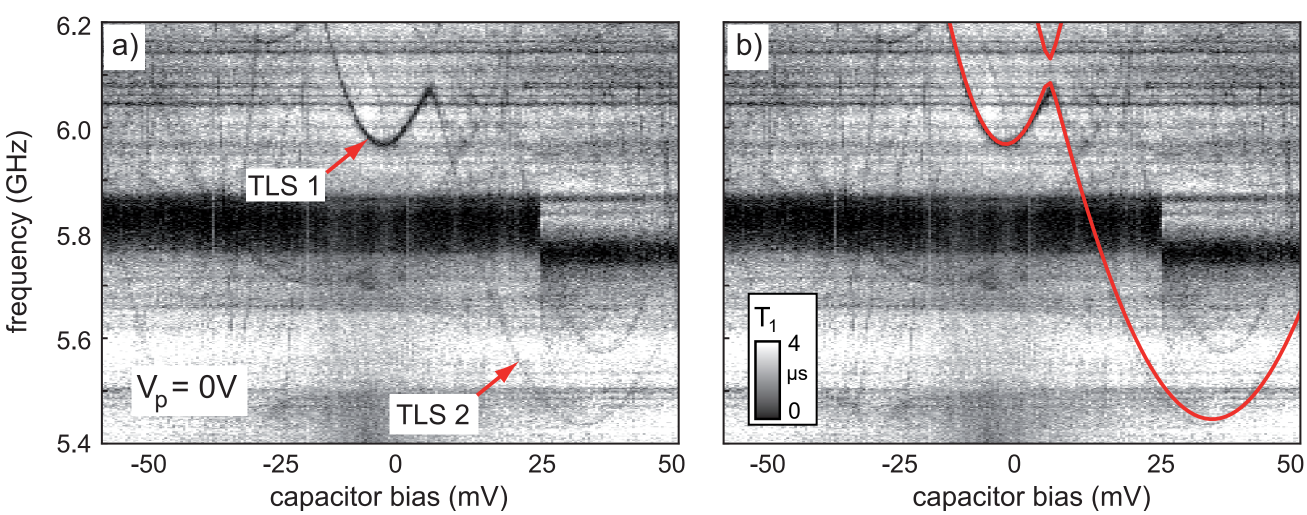

FIG. **S2**. Swap-spectroscopy of the interacting TLS system in a wider frequency range, obtained at $V_\mathrm{p} = 0$V. **a)** Raw data, where the arrows indicate the traces of TLS 1 and TLS 2. **b)** Same data with superimposed fits calculated with the extracted TLS parameters shown in Table I.

parameter			**TLS 1**	**TLS 2**
tunnel energy	Δ_i	(GHz)	5.957	5.440
local field coupling	$\gamma_{\mathrm{s},i}$	(GHz/V_s)	161.95	92.25
el. dipole moment	$p_\parallel$	(eÅ)	0.335	0.191
strain coupling	$\gamma_{\mathrm{p},i}$	(MHz/V_p)	22	0

TABLE I. Parameters of the interacting TLS, obtained by fitting the data shown in Fig. 3 of the main text and the data shown in Fig. **S2**. For TLS 2, no strain dependence could be detected.

Deposition of alignment marks

To minimize contamination and manufacturing time, the niobium alignment marks, which were required for the electron-beam lithography, were deposited on the same resist mask that was used to etch the main structures into the Al film. During Nb deposition, the main structures were covered with a protecting wafer as further detailed in the PhD thesis by AB, Chap. 3.2.1[2].

SUPPLEMENTARY FIGURES

Figure **S3** and Fig. **S4** show complete data sets recorded on nominally identically Qubits #1 and #2, respectively.

SUPPLEMENTARY NOTES

The here discussed work was part of the PhD studies of Alexander Bilmes at Karlsruhe Institute of Technology (KIT). Further details on the experimental setup, electric field simulations, and data acquisition can be found in his thesis[2].

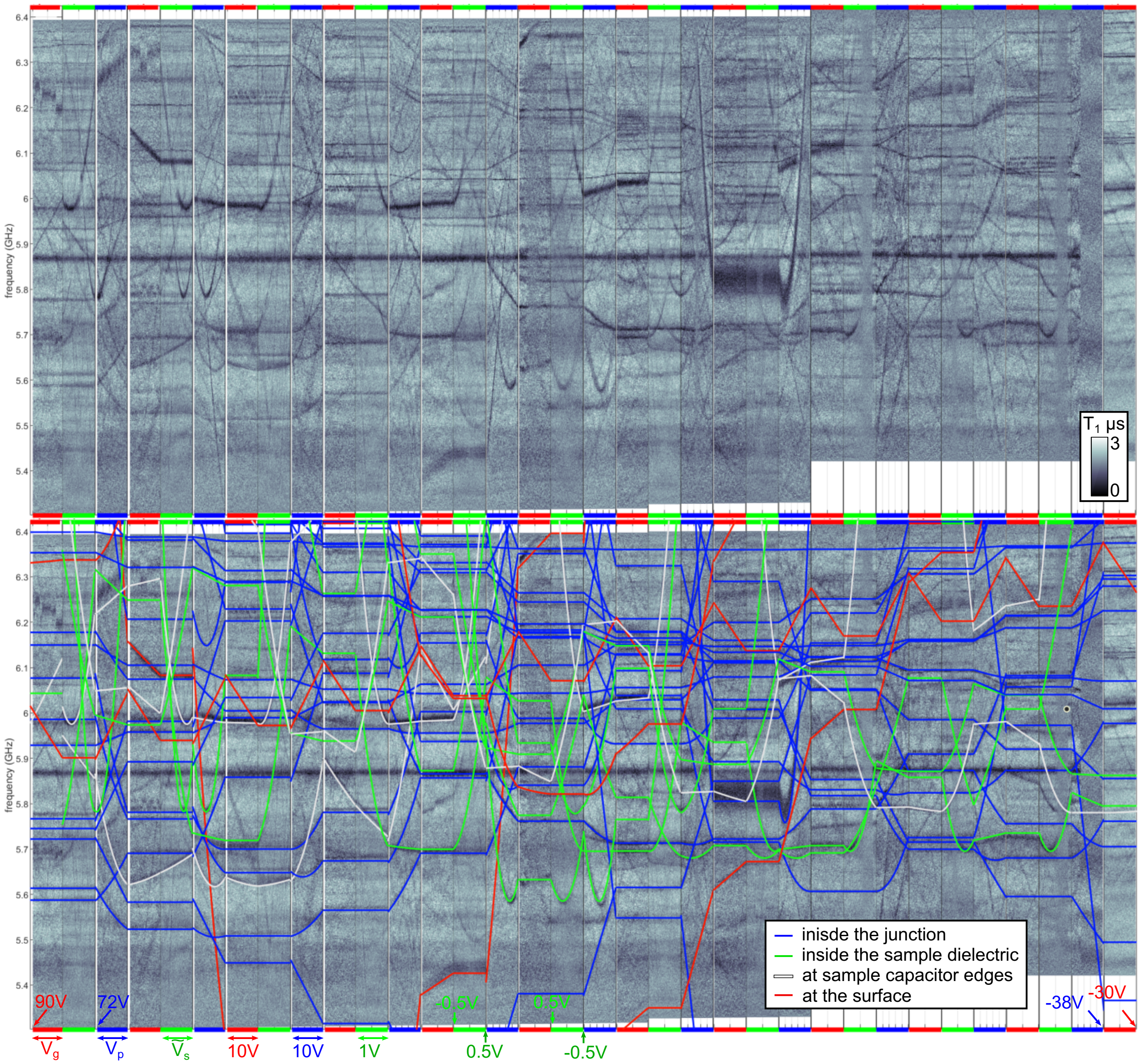

FIG. **S3**. Swap-spectroscopy data to measure the response of TLS to the global DC-electric field controlled by V_g (red framed segments), to the local field applied directly to the capacitor electrode via the voltage $\widetilde{V}_s$ (green segments), and to mechanical strain controlled by the piezo voltage V_p (blue). Top panel: raw data, bottom panel: with superimposed hyperbolic fits to the TLS' resonance frequencies. While V_g and V_p were both ramped linearly down from about 90V to -30V, $\widetilde{V}_s$ was ramped alternatingly up or down with the amplitude limited to $|\widetilde{V}_s| < 0.5$V to avoid heating of the attenuators. Data recorded on qubit #1.

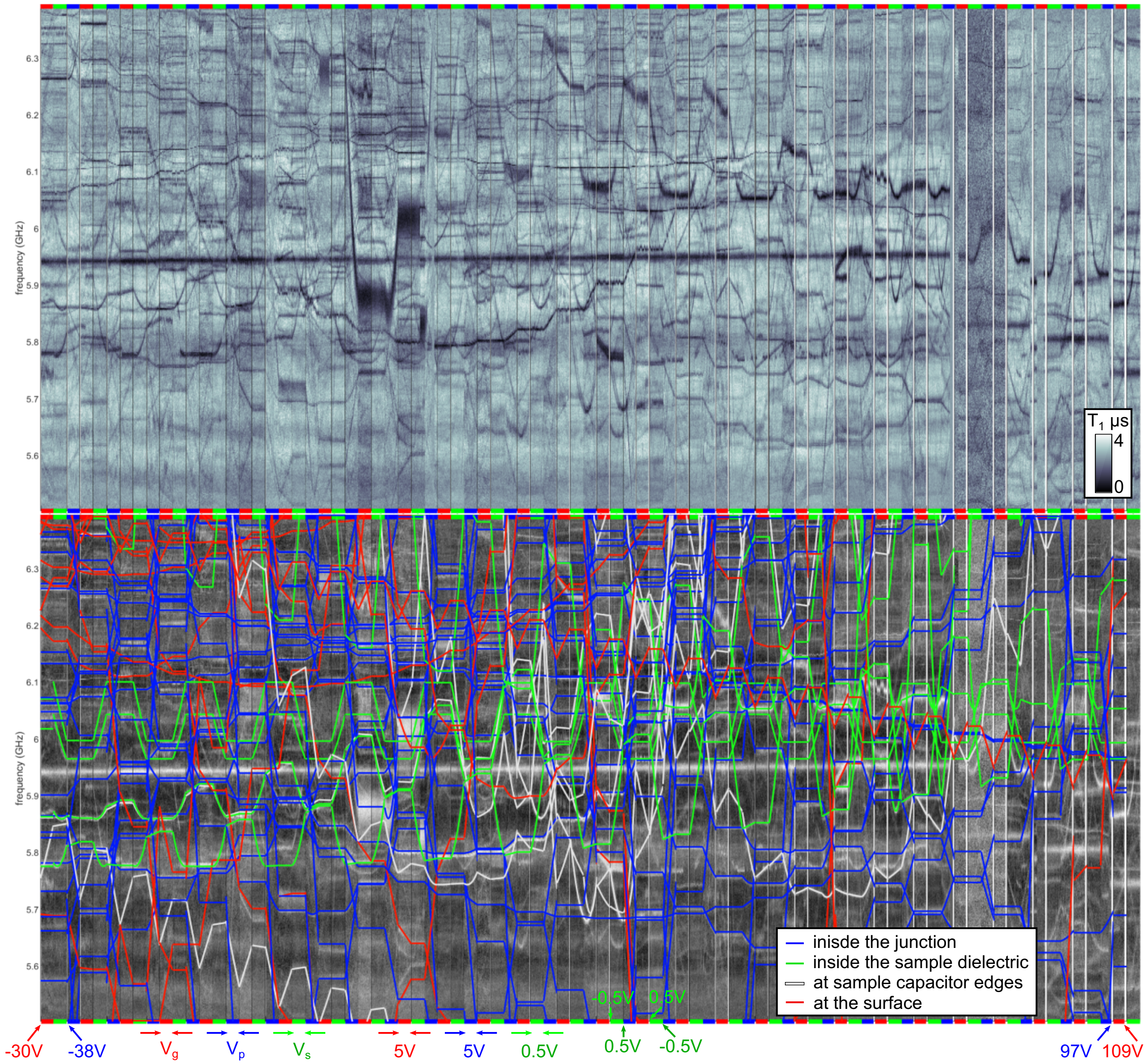

FIG. **S4**. Top panel: Raw swap-spectroscopy data recorded on Qubit #2 in a similar manner as Fig. **S3**. Bottom panel: same data with superimposed fits.

SUPPLEMENTARY REFERENCES

[1] Martinis, J. M. *et al.* Decoherence in Josephson qubits from dielectric loss. *Physical Review Letters* **95**, 210503 (2005).
[2] Bilmes, A. *Resolving locations of defects in superconducting transmon qubits*. dissertation, Karlsruhe Institute of Technology (KIT) (2019). URL `http://dx.doi.org/10.5445/KSP/1000097557`.
[3] Sarabi, B., Ramanayaka, A. N., Burin, A. L., Wellstood, F. C. & Osborn, K. D. Projected dipole moments of individual two-level defects extracted using circuit quantum electrodynamics. *Phys. Rev. Lett.* **116**, 167002 (2016).
[4] Brehm, J. D., Bilmes, A., Weiss, G., Ustinov, A. V. & Lisenfeld, J. Transmission-line resonators for the study of individual two-level tunneling systems. *Applied Physics Letters* **111**, 112601 (2017).
[5] Lisenfeld, J. *et al.* Observation of directly interacting coherent two-level systems in an amorphous material. *Nat Commun* **6**, 6182 (2015).
[6] Johansson, J. R., Nation, P. D. & Nori, F. "qutip 2: A python framework for the dynamics of open quantum systems.". *Comp. Phys. Comm.* (2013).